International Journal of Thermal Sciences 49 (2010) 1063–1071

Contents lists available at ScienceDirect

International Journal of Thermal Sciences

journal homepage: www.elsevier.com/locate/ijts

Experimental fouling investigation with electroless Ni–P coatings

A. Al-Janabi [a,1], M.R. Malayeri [a,*], H. Müller-Steinhagen [a,b,2]

[a] Institute for Thermodynamics and Thermal Engineering (ITW), University of Stuttgart, Pfaffenwaldring 6, 70550 Stuttgart, Germany
[b] Institute for Technical Thermodynamics, German Aerospace Centre, Pfaffenwaldring 38-40, 70569 Stuttgart, Germany

ARTICLE INFO

Article history:
Received 15 December 2008
Received in revised form
26 February 2009
Accepted 25 May 2009

Keywords:
Modified surfaces
Coating
Surface energy
Fouling
Calcium sulphate

ABSTRACT

Advanced fouling mitigation techniques include approaches to increase the duration of the induction period and/or to decrease the fouling rate during the deposition process. One such technique is to generate heat transfer surfaces with high repulsive forces to make them less attractive to the deposition of dissolved or suspended matter. The present work investigates and compares different electroless Ni–P coatings with or without boron-nitride (BN). The incorporation of boron-nitride into Ni–P coatings increases the electron donor component of surface energy which in turn reduces the propensity of the coating to fouling. A systematic set of fouling runs has been conducted to investigate the influence of these coatings on the interaction energies between $CaSO_4$ deposits and modified surfaces. The results show that the Ni–P coatings with Boron-nitride exhibit excellent anti-fouling behaviour compared to pure Ni–P coatings or untreated stainless steel surfaces. Surfaces having a higher electron donor component in case of Ni–P–BN produce a higher repulsive energy which causes the adhesion force between the surface and deposits to decrease. A simultaneous set of reproducibility and cleanability experiments, however, reveals that the observed surface properties of the investigated coatings are prone to significant aging after each fouling run, leading to poor abrasion resistance.

1. Introduction

Heat exchanger fouling is a severe industrial problem in which the accumulation of materials with low thermal conductivity acts as barrier to heat transfer. It is also a very complex process in which many parameters are involved such as i) operating conditions, ii) feed composition, iii) geometry of heat exchanger, and iv) surface properties. In recent years, technological advancements have given new impetus to producing innovative modified surfaces with better anti-fouling characteristics [1]. The pivotal notion here is to modify the surface energy such that the formation of crystals onto the surface can be reduced as the poorest fouling adhesion occurs on materials with lower surface energies [2].

Polymer coatings such as PTFE have been studied due to their low surface energy and non-sticking properties [3]. However, the main disadvantages of such coatings are the weak abrasion resistance and the poor heat transfer characteristics. The incorporation of PTFE nanoparticles into a Ni–P matrix produces metal based coatings which can substantially overcome some of these shortcomings [4]. Zhao et al. [5] showed that the surface energy of Ni–P–PTFE has a dominant influence on microstructure and adhesion of the resulting $CaSO_4$ scale deposits The incorporation of copper into the electroless Ni–P matrix may further improve the thermal performance of the coatings [6]. The resulting electroless Ni–Cu–P–PTFE coating strongly affects the adhesion of $CaSO_4$ deposits onto the surfaces, as shown in Fig. 1. Zhao et al. [7] also showed that the lowest adhesion of $CaSO_4$ deposits occurred when the surface free energy was around 26–30 mN/m.

The present study endeavors to investigate Ni–P coatings which are fortified with boron-nitride in order to enhance the repulsive forces on the surface. In addition, the coatings have a better thermal stability than PTFE coatings. The Ni–P coatings have systematically been subjected to fouling from supersaturated $CaSO_4$ solutions during convective heat transfer. The findings of this investigation may contribute to the understanding of the characteristics of crystallization fouling on electroless Ni–P coatings, particularly of the relationship between deposition mechanisms and surface energy properties.

2. Coating characteristics

Coating characterizations were carried out prior to each fouling run to determine the coating properties in terms of surface roughness, contact angle, and surface energy. The base substrates

Abbreviations: PTFE, Poly-Tetra-Fluoro-Ethylene; BN, Boron-Nitride.

* Corresponding author. Tel.: +49 711 68567656; fax: +49 711 68563503.
E-mail addresses: herz@itw.uni-stuttgart.de (A. Al-Janabi), m.malayeri@itw.uni-stuttgart.de (M.R. Malayeri), hans.mueller-steinhagen@dlr.de (H. Müller-Steinhagen).
[1] Tel.: +49 711 68563254; fax: +49 711 68563503.
[2] Tel.: +49 711 6862358; fax: +49 711 6862712.

1290-0729/$ – see front matter © 2009 Elsevier Masson SAS. All rights reserved.
doi:10.1016/j.ijthermalsci.2009.05.009

Nomenclature

c	Concentration, g/L
f	Friction coefficient
ΔG_{132}^{TOT}	Total interaction energy, mN/m
ΔG_{132}^{LW}	Lifshitz–van der Waals interaction energy, mN/m
ΔG_{132}^{AB}	Lewis acid-base interaction energy, mN/m
ΔG_{132}^{EL}	Electrostatic double layer interaction energy, mN/m
ΔG_{132}^{Br}	Brownian motion energy, mN/m
$\dot{q}$	Heat flux, W/m ^{2}
R_f	Fouling resistance, m^2 K/W
T	Temperature, °C
t_{ind}	Induction time, min
U	Overall heat transfer coefficient, W/m^2 K
ν	Velocity, m/s
ν^*	Shear velocity, m/s

Greek symbols

γ_{12}	Solid/liquid interface free surface energy, mN/m
γ_2	Solid/vapour interface free surface energy, mN/m
γ_3	Liquid/vapour interface free surface energy, mN/m
γ^{LW}	Non-polar, dispersive component of surface energy, mN/m
γ^{AB}	Polar component of surface energy, mN/m
γ^+	Electron acceptor component of surface energy, mN/m
γ^-	Electron donor component of surface energy, mN/m
θ	Contact angle, degree

Subscript

0	time zero or clean condition
b	bulk

were all of AISI 304 BA stainless steel with 50 mm × 59 mm area and 0.3 mm wall thickness. The surfaces were coated with electroless Ni–P coatings with or without boron-nitride (BN), which were provided by NovoPlan GmbH, Aalen, Germany. The first coating consists of 50 μm of Ni–P with 7–9% P (phosphor). The second coating (Ni–P–BN) consists of two layers. The first layer consists of 40 μm of Ni–P with 7–9% P and the second layer on top is made from 10 μm of BN (Ni–P with 12–15% boron-nitride). This is because the present technology of the coating company is limited to a maximum coating thickness of "only Ni–P–BN" 15 μm. Thus an additional layer of Ni–P is applied below the second layer in order to realise an identical thickness of 50 μm for both coatings of Ni–P and Ni–P–BN (Table 1).

2.1. Surface roughness

The most commonly used roughness parameter, i.e. the mean roughness profile (R_a) was determined by using a stylus instrument (Perthometer M4Pi, Mahr, Germany) over a length of 15 mm in three horizontal and vertical lines, respectively. As listed in Table 2, the variation of surface roughness between the various coatings is only marginal and would hence not affect the investigated deposition mechanisms. To validate this, the shear velocity ($v^* = v(f/2)^{1/2}$) is determined and tabulated in Table 2, showing only negligible variations.

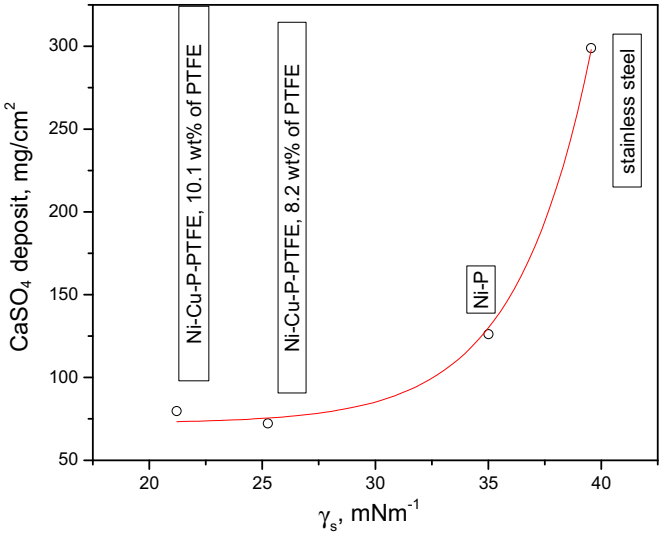

Fig. 1. Effect of the surface free energy on $CaSO_4$ scale formation (Zhao et al. [5]).

2.2. Contact angle and surface energy

An important parameter influencing the adhesion of deposit on modified surfaces is the free surface energy. It provides a direct measure of the interfacial attractive forces. The common relationship for the characterisation of surfaces with respect to surface energy is the Young equation [8]. This equation describes the force balance, as shown in Fig. 2, between a solid surface, a drop of liquid placed on it and the surrounding atmosphere:

$$\gamma_{12} = \gamma_2 - \gamma_3 \cos\theta \tag{1}$$

Several thermodynamic approaches are available to determine the surface energy of a solid surface. In this work, the adhesion of deposits obtained in the laboratory has been analyzed by the Lewis acid/base approach which focuses on the electron donor component and its significant effect on the fouling process. The approach was developed by van Oss et al. [9,10] and is based on the total surface energy of a solid which is the sum of a non-polar Lifshitz–van der Waals (*LW*) force component γ^{LW}, and a polar Lewis acid/base force component γ^{AB}:

$$\gamma_i = \gamma_i^{LW} + \gamma_i^{AB} \tag{2}$$

The acid-base polar component can be further subdivided into electron donor (γ^-) and electron acceptor (γ^+) interaction components as:

$$\gamma_i^{AB} = 2\sqrt{\gamma_i^+ \gamma_i^-} \tag{3}$$

The solid/liquid interface energy is then given by

$$\gamma_{12} = \gamma_2 + \gamma_3 - 2\left(\sqrt{\gamma_2^{LW} \cdot \gamma_3^{LW}} + \sqrt{\gamma_2^+ \cdot \gamma_3^-} + \sqrt{\gamma_2^- \cdot \gamma_3^+}\right) \tag{4}$$

where 1, 2, and 3 indicate the deposit, substrate and liquid, respectively.

Table 1
Compositions (wt. %) of Ni–P coatings.

Component	Ni–P	Ni–P–BN
P (phosphorus)	7–9	7–9
BN (boron-nitride)	–	12–15

Table 2
Surface energy components of electroless Ni–P coating, untreated surfaces, $CaSO_4$, and water.

Surface	R_a, μm	Shear velocity, v^*	Surface energy components, mN/m		
			γ^{LW}	γ^+	γ^-
Ni–P	0.18	0.00862	40.68	0.84	16.64
Ni–P–BN	0.21	0.00863	45.55	0.45	25.3
SS	0.3	0.00865	35.11	0.03	3.46
$CaSO_4{\cdot}2H_2O$ [26]	–	–	35	0.01	44
Water	–	–	21.8	25.5	25.5

Combining this with the Young Eq. (1), a relation between the measured contact angle and the solid and liquid surface free energies can be obtained:

$$\gamma_3\cdot(1+\cos\theta) = 2\left(\sqrt{\gamma_2^{LW}\cdot\gamma_3^{LW}}+\sqrt{\gamma_2^+\cdot\gamma_3^-}+\sqrt{\gamma_2^-\cdot\gamma_3^+}\right) \quad (5)$$

In order to determine the surface free energy components (γ_2^{LW}) and the parameters γ_2^+ and γ_2^- of a solid material, the contact angles of at least three liquids, e.g. distilled water, diiodomethane and ethylene glycol with known surface tension components ($\gamma_3^{LW}, \gamma_3^+$ and γ_3^-), have to be determined. Table 2 lists various values of these components. It can be seen that Ni–P–BN coating increases the surface free energy by approximately (29%) above that of the untreated stainless steel surface. The main effect of the electroless Ni–P coatings is to increase the electron donor component of the surface energy. The surface energy and its components, such as the electron donor component, may be indicative of the propensity of a surface to foul or not. However the magnitude of adhesion between incrustation and surface and its growth rate is directly related to the work of adhesion which in turn depends on surface energy according to:

$$W_a = \gamma_2+\gamma_3-\gamma_{12} \quad (6)$$

2.3. Deposit/surface adhesion energies

In the classical nucleation theory proposed by Mullin [11] the tendency of a crystal to grow depends on two thermodynamics factors. The first is the driving force for crystallization which is expressed as the Gibbs free energy of transfer from a supersaturated to an assumed saturated solution at the interface. The second is the energy barrier for integration of ions into a crystal lattice that can be treated as a physico-chemical interaction force resulting from the total interaction energy between a deposit and a metal surface.

Since in the present work, the supersaturation of the solution and its flow velocity were kept constant, the formation of deposits could be attributed to the interaction between the deposit and the solid surface. Fig. 3 gives an overview of the interaction energies which may affect the process of adhesion. According to the DLVO theory named after Derjaguin, Landau, Verwey and Overbeek, the principal interaction energies are determined by the balance

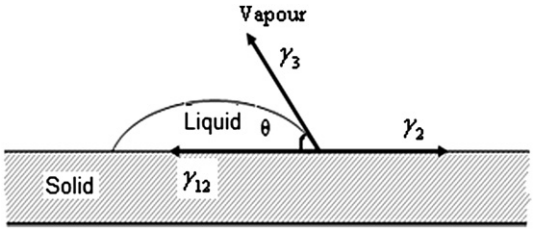

Fig. 2. Interfacial free energies at the boundaries between three phases.

between i) the attractive Lifshitz–van der Waals energy (LW) which basically depends on the geometry and on the physical/chemical properties of the interacting bodies, and ii) the repulsive double layer energy due to the tendency of particular materials to acquire an electrical charge when immersed in a polar medium. In a polar medium (e.g. water), Lewis acid-base interaction can cause anomalies in the theoretical interpretation of interfacial interactions according to the DLVO theory, as they can exceed the DLVO energies by as much as two orders of magnitude [12]. Hence van Oss [13] extended the DLVO theory by including the Lewis acid-base interaction energy (*AB*). In addition to these interaction energies, crystals may be adhering to a surface due to the effect of Brownian motion (*Br*), which will bring the precursor materials into contact with the surface in question. Thus, the total interaction energy ΔG_{132}^{TOT} between a deposit and a solid surface can be written as the sum of the various interaction energies [12,13].

It should be furthermore considered, that substantial adhesion and growth of deposits can only occur if the flow of the liquid is not able to provide a shear force strong enough to overcome the attractive force between crystals and the solid surface. However, modelling this additional effect is not part of the present investigation.

$$\Delta G_{132}^{TOT} = \Delta G_{132}^{LW}+\Delta G_{132}^{EL}+\Delta G_{132}^{AB}+\Delta G_{132}^{Br} \quad (7)$$

Oliveira [13] suggested that the balance between all possible interactions between a deposit and a metal surface determines whether a system will foul or not, i.e. adhesion/fouling will take place if ΔG_{132}^{TOT} is negative. In many systems, the electrostatic interactions and the effect of Brownian motion can be neglected [14]. In this case Eq. (7) can be expressed as:

$$\Delta G_{132}^{TOT} = \Delta G_{132}^{LW}+\Delta G_{132}^{AB} \quad (8)$$

The Lewis acid-base energy ΔG_{132}^{AB} is mainly a function of i) $\Delta G_{132(H_o)}^{AB}$ which represents the free energy at the equilibrium distance (H_o), and ii) the actual distance (H) between interacting bodies [15].

Basically, H_o is defined as the minimum equilibrium distance between the two interacting bodies, which has been found for a large range of materials to be equal to 0.157 nm [12]. By assuming H to be equal to H_o [16], ΔG_{132}^{AB} becomes only a function of the γ^- and γ^+ values of the polar component of the surface energy of the interacting bodies. If a calcium sulphate crystal (1) interacts with a heat transfer surface (2) when immersed in a polar medium, such as water (3), the polar component of ΔG_{132}^{AB} is expressed by

$$\Delta G_{132}^{AB} = 2\left(\sqrt{\gamma_2^+\gamma_3^-}+\sqrt{\gamma_1^+\gamma_3^-}-\sqrt{\gamma_3^+\gamma_3^-}+\sqrt{\gamma_2^-\gamma_3^+}+\sqrt{\gamma_1^-\gamma_3^+}-\sqrt{\gamma_3^+\gamma_3^-}-\sqrt{\gamma_2^+\gamma_1^-}-\sqrt{\gamma_2^-\gamma_1^+}\right) \quad (9)$$

As a result, Eq. (8) can be transformed into:

$$\Delta G_{132}^{TOT} = 2\left(\sqrt{\gamma_2^{LW}\gamma_3^{LW}}+\sqrt{\gamma_1^{LW}\gamma_3^{LW}}-\sqrt{\gamma_2^{LW}\gamma_1^{LW}}-\gamma_3^{LW}\right)+2\left(\sqrt{\gamma_2^+\gamma_3^-}+\sqrt{\gamma_1^+\gamma_3^-}-\sqrt{\gamma_3^+\gamma_3^-}+\sqrt{\gamma_2^-\gamma_3^+}+\sqrt{\gamma_1^-\gamma_3^+}-\sqrt{\gamma_3^+\gamma_3^-}-\sqrt{\gamma_2^+\gamma_1^-}-\sqrt{\gamma_2^-\gamma_1^+}\right) \quad (10)$$

If the various components of the surface free energy of calcium sulphate, heat transfer surface and water are known (see Table 2), then ΔG_{132}^{TOT} can be calculated as presented in following sections.

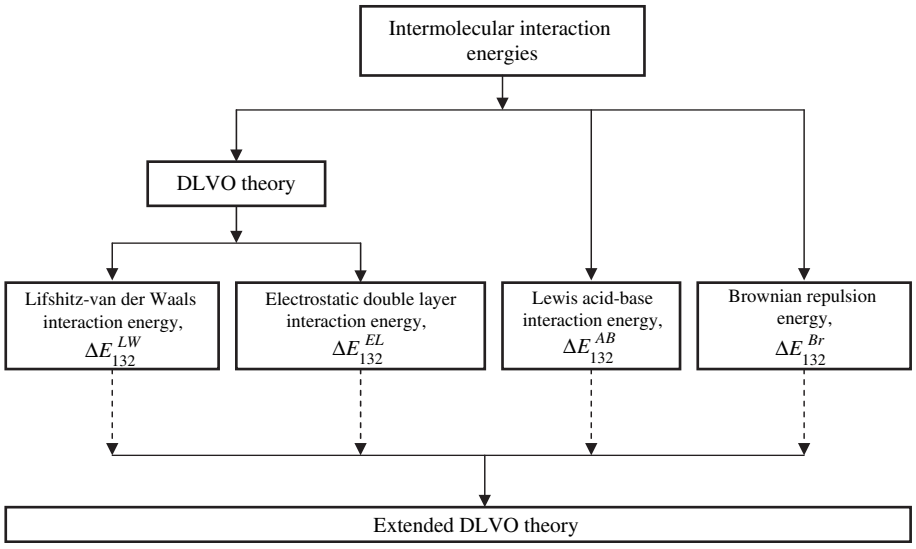

Fig. 3. Molecular interaction energies influencing adhesion.

3. Experimental set-up and procedure

3.1. Test rig and data acquisition

The investigation of fouling on coated surfaces during convective heat transfer was performed using the experimental apparatus which is schematically represented in Fig. 4. The closed loop set-up consists of two vertical rectangular ducts operated in parallel. On both sides of each duct, openings with the size of 59 mm × 50 mm exist where the modified surfaces can be mounted. The heated zone of the modified surfaces is positioned 1.5 m upstream of the duct inlet. This arrangement provides fully developed turbulent flow. Using a centrifugal pump, the solution is pumped from a 47 l stainless steel tank through a 12 μm filter to remove any broken

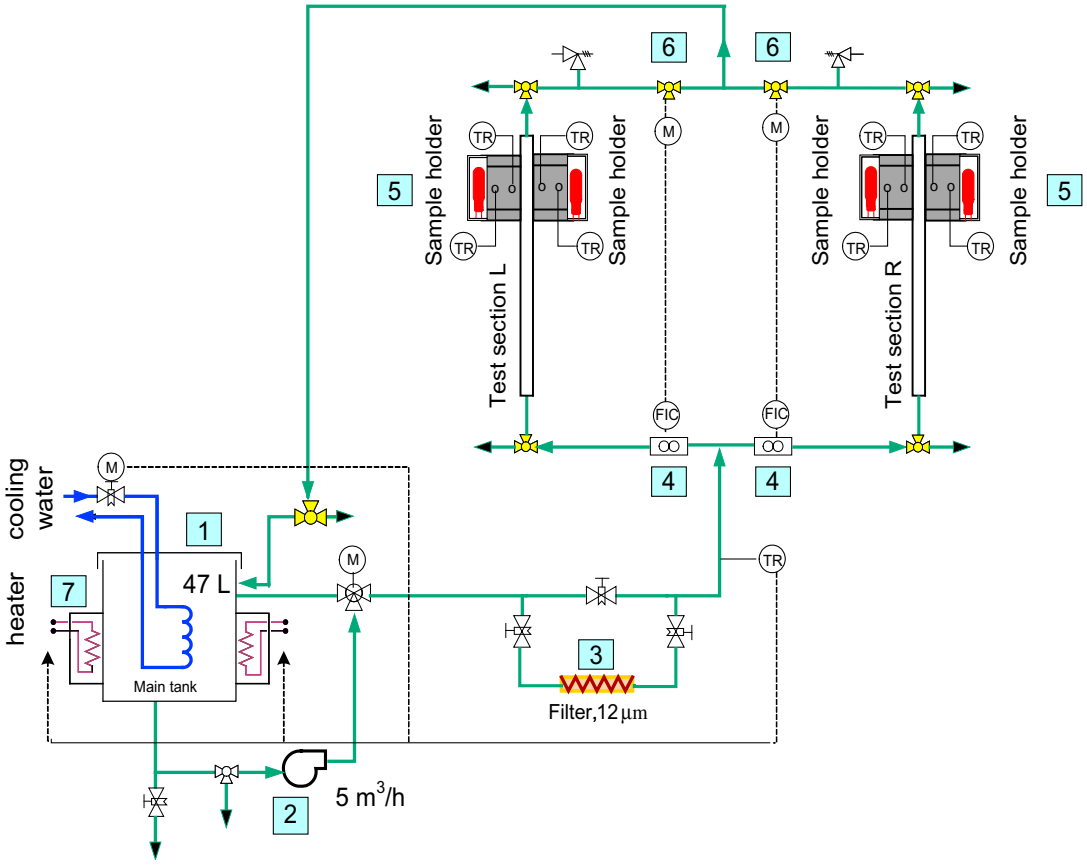

Fig. 4. Schematic diagram of experimental set-up.

crystals and impurities from the solution, which might artificially act as nucleation sites. The filter is 0.5 m long and made of polypropylene and polyethylene. Subsequently, the flow is divided into two equal streams in the left and right ducts as shown in Fig. 4. The flow rate is kept constant and controlled separately using two magnetically inductive flow meters in conjunction with PID automatic controllers and two electrically controlled valves. The two partial flows are recombined after the heated zone and fed back to the storage tank. To avoid pump damage and to have better flow control a bypass pipe system from the pump back to the tank has been installed. The temperature of the solution in the tank was regulated using a water-cooled coil inside the tank, together with two heater pads installed on the outer surface of the tank. The heat transfer specimens, as schematically shown in Fig. 5, are of 0.3 mm thickness with 59 mm × 50 mm area, on which two copper blocks (40 mm × 20 mm) were vacuum-soldered as shown in Fig. 5. The specimens are heated by using two 450 W golden infrared heaters (Heraeus Noblelight GmbH, Hanau, Germany), which are radiated by a sight glass on the back of the copper blocks. The attainable heat flux at the specimen surface is about 100 kW/m^2. During each experiment, the transmitted heat flux from the surfaces is measured and regulated by means of automatic PID controlled dimmers with a maximum deviation from the desired value of less than ±4.8%.

A graphical programming language "VEE pro 6" (Agilent Technologies GmbH, Böblingen, Germany) was used to record and process all experimental data such as flow rate, bulk temperature, heat flux, and the temperature of the heat transfer surfaces. The analysis of the measured data took place on a separate PC where the outcomes are stored in Excel spreadsheets. For a better evaluation of the system, the measured temperature time series are plotted as a graphical view with a time interval of 26 s.

3.2. Test solution

Calcium sulphate solution is used as foulant in this study. It is prepared by directly dissolving calcium nitrate tetrahydrate, $Ca(NO_3)_2 \cdot 4H_2O$, and sodium sulphate, Na_2SO_4 in distilled water as per Eq. (11). The two chemicals were initially dissolved separately in 23.5 l of distilled water and mixed together in a 47 l stainless steel tank in such a way that the desired $CaSO_4$ concentration is achieved.

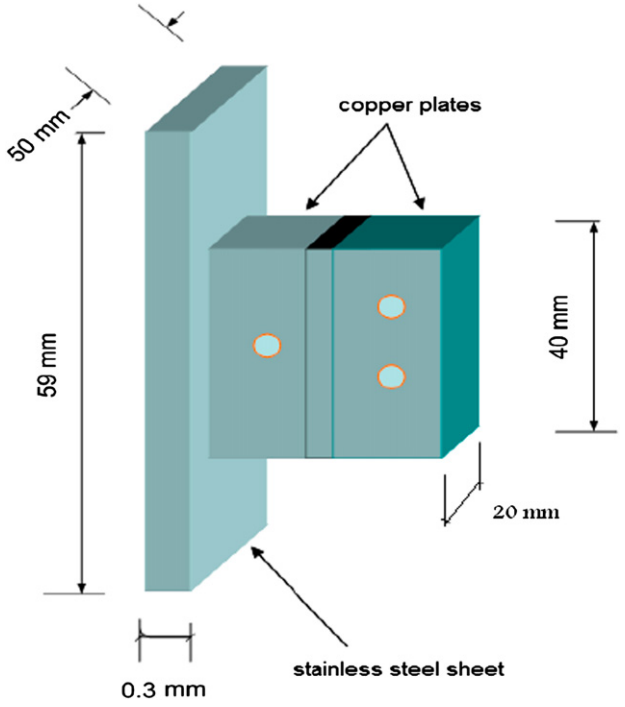

Fig. 5. Heat transfer specimen.

$$Ca(NO_3)_2 \cdot 4H_2O + Na_2SO_4 \rightarrow CaSO_4 + 2NaNO_3 + 4H_2O \qquad (11)$$

3.3. Experimental procedure

All modified surfaces were initially washed with toluene, then rinsed with water to remove any remaining contamination and immediately after that mounted in the rig to commence a fouling run. Then the selected heat flux, bulk temperature and fluid velocity are adjusted and the rig started to operate under clean conditions with distilled water until steady-state is reached, i.e. the temperatures indicated by the thermocouples remain unchanged. During this period the test solution is prepared and heated to the desired value (40 °C). After 2 h of steady-state operation, the test run is stopped, the distilled water removed and replaced by the test solution. The solution is then circulated for about 10 min with the heaters off, to ensure that any dissolved air can find its way to de-aerators which have been mounted on the top of the supply tank and leave the system from. Subsequently, the power supply to the surfaces is switched on and the data collection started. During the experiment the Ca^{2+}-ion concentration is determined by EDTA-titration every 2–3 h and adjusted by adding equimolar calcium nitrate tetrahydrate and sodium sulphate to maintain a constant $CaSO_4$ concentration of 4 g/L. However such adjustment is less than 5% during the first 3 h of the fouling runs. This is a result of the relatively large size of the supply tank, which prevent rapid reduction of concentration when the solution is continuously circulated. The chemical adjustment may lead to increased concentrations of other ions such as NO_3 and Na in the solution which increase the solubility of calcium sulphate [17]. Nevertheless, systematic tests in the same test rig have shown that the effect of such ions on the fouling behaviour is negligible [18]. Once the surface temperature reached a set limit (typically 160 °C) the heating was automatically stopped and the all measured data stored in an output file.

3.4. Error analysis

The impact of systematic and experimental errors has been determined with a 95% confidence interval. The systematic experimental errors in the determination of heat transfer coefficients and fouling resistances are due to i) errors of approximately ±0.2 °C in temperature measurement and ii) an error of about 4.8% for the determination of heat flux. The uncertainty of both heat transfer coefficients and fouling resistances varies with time due to change in surface temperature once the layer of incrustation starts to build up on the heat transfer surface. For instance, the uncertainty of the fouling resistance for a typical fouling run with 100 kW/m^2 heat flux, 40 °C bulk temperature, and 4 g/L $CaSO_4$ concentration changes from 44.73% to 4.9% as time is goes on. This indicates that the largest experimental uncertainty of the fouling resistance occurs at the beginning of the experiments when the difference between initial and actual heat transfer surface temperature is still small.

4. Experimental results and discussion

4.1. Fouling resistance and deposition of $CaSO_4$ on Ni–P coatings

One of the main indicative parameters for the deposition process is the fouling resistance which quantitatively

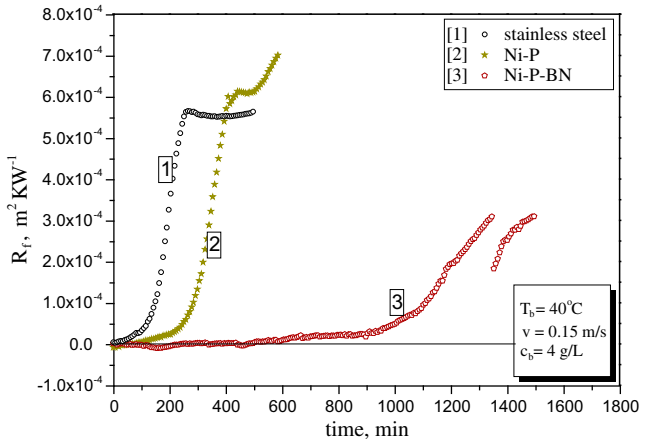

Fig. 6. Fouling resistance as a function of time for untreated and electroless Ni–P coated surfaces.

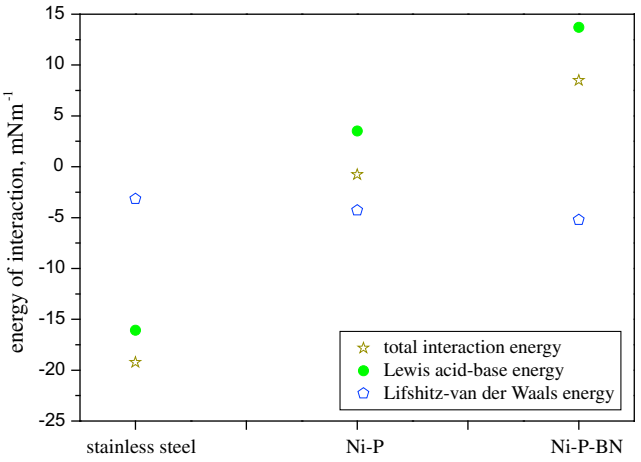

Fig. 8. Interaction energies for coated and untreated surfaces.

represents the reduction of heat transfer coefficient as a function of time:

$$R_f = \frac{1}{U_t} - \frac{1}{U_0} \tag{12}$$

In this equation "U" is the overall heat transfer coefficient and subscripts "t" and "0" denote conditions at any time and at the beginning of the experiment, when the heat transfer surface is considered to be clean. In any fouling resistance curve as shown in Fig. 6, two important features are of particular interest 1) induction time, i.e. the time that elapses before the increase in fouling resistance become notable and 2) the fouling rate which is the slope of the fouling curve in the region where the fouling resistance increases continuously. Fig. 6 demonstrates that the electroless Ni–P surfaces reduce the fouling resistance significantly in comparison with untreated stainless steel surfaces.

It is evident that the Ni–P–BN surface has a considerably different fouling behaviour than the Ni–P and untreated surfaces. Clearly, the induction time for Ni–P–BN is significantly longer than for the other two surfaces. Furthermore, visual observations during the fouling runs showed that after a certain period of time the $CaSO_4$ deposits on the Ni–P–BN surface tended to break-off. Furthermore, as indication for the affinity of the surfaces for calcium sulphate deposition, the initial fouling rate was used. It is apparent that the Ni–P–BN coating experiences smaller amounts of deposit in comparison to the other two surfaces (Ni–P and untreated stainless steel Fig. 7).

The impact of different coatings on the fouling behaviour can be attributed to the varying interaction between the molecules on the surface and the ions in the solution. For the Ni–P–BN coatings, the higher values of the electron donor component in the surface energy may imply that the deposition process is much slower than for the other two surfaces that have been investigated simultaneously. Alternatively, the difference in fouling tendency may be attributed to the influence of deposit/heat transfer surface interfacial energy. Fig. 8 indicates that the contribution of ΔG_{132}^{AB} to the total interaction energy ΔG_{132}^{TOT} is higher to that of the Lifshitz–van der Waals energy ΔG_{132}^{LW}. Thus for the investigated modified surface in this study, the variation of ΔG_{132}^{AB} may be the major indicative whether a surface fouls or nor while the impact of ΔG_{132}^{LW} to the total interaction energy is only marginal.

The electron donor component of the surface energy may also be directly related to difference in fouling tendency on modified surfaces. Surfaces having a relatively high value of electron donor component (γ^-) have been found to cause a reduction of the total interaction energy [19]. This is indeed expected to inhibit the crystal growth due to total interaction energies across the interface as shown in Fig. 9. In this figure for higher values of the electron

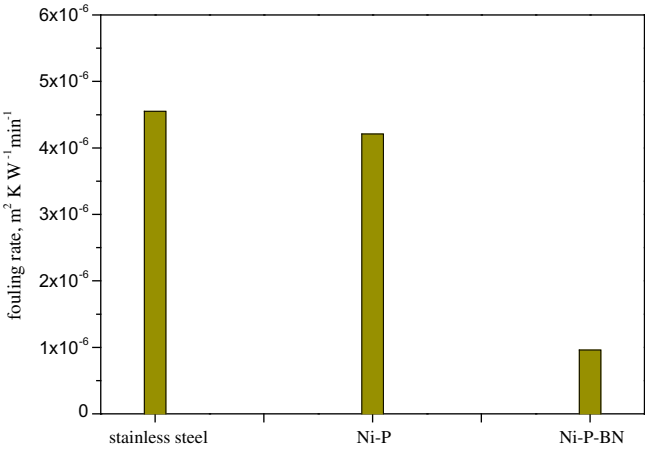

Fig. 7. Initial fouling rate of electroless Ni–P, Ni–P–BN and untreated stainless steel surfaces.

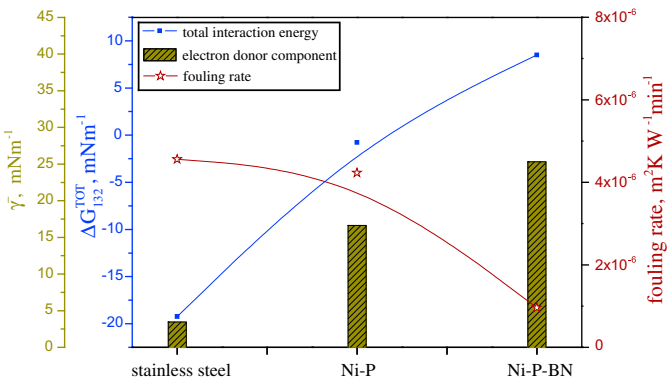

Fig. 9. Initial fouling rate as a function of total interaction energy and electron donor component of stainless steel and coated surfaces.

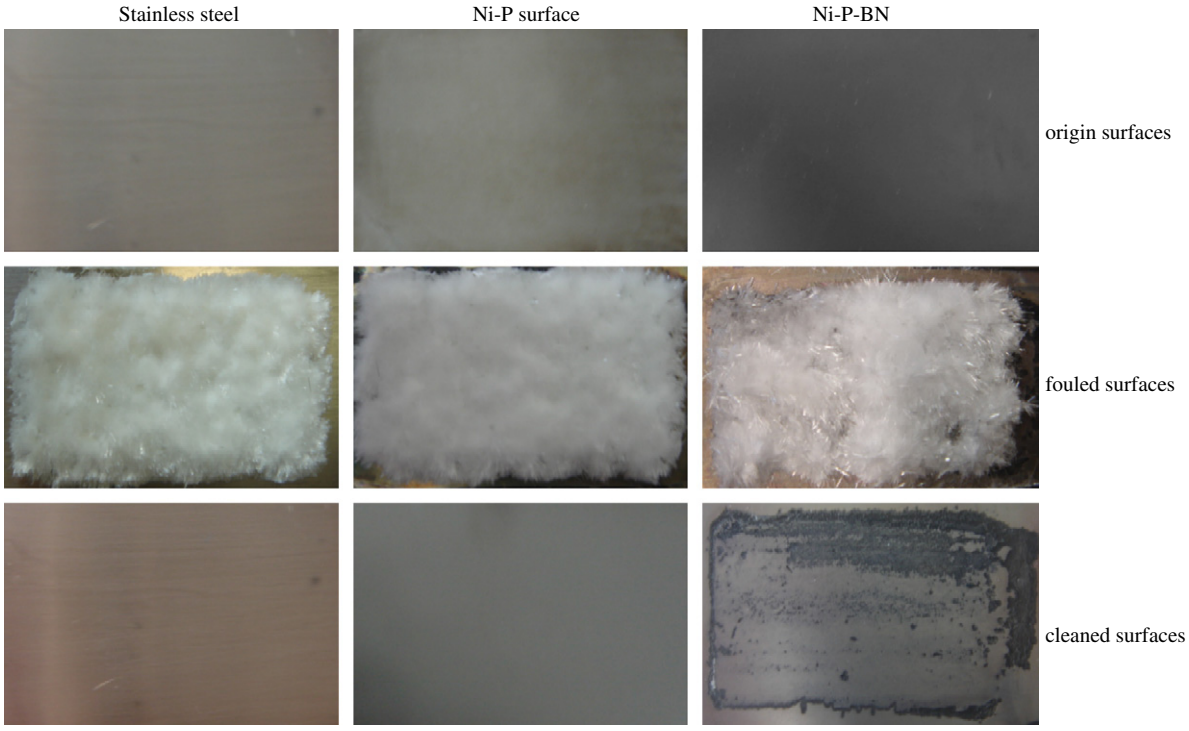

Fig. 10. Clean and fouled electroless Ni–P and stainless steel surfaces for $T_b = 40\ ^\circ C$, $v = 0.15$ m/s, heat flux $= 100$ kW/m^2 and $c_b = 4$ g/L.

donor component of surface energy also ΔG_{132}^{TOT} increases simultaneously. These findings are consistent with those of Visser [19] who showed that an important parameter to reduce calcium phosphate fouling is to increase the electron donor component of the surface energy. However, there are numerous studies where different conclusions have been derived, even though for different foulants. For example, the deposition rate of calcium phosphate was found to increase with increasing γ^- [20–22]. Wu and Nancollas [20] stated that the effect of the interaction energies on calcium phosphate deposition is dominated by the high value of the Lewis acid-base and electrostatic energies. Nevertheless, i) the contribution of the electrostatic energy in most cases (especially in aqueous solutions) can be considered as a repulsive interaction energy [23] or can be neglected altogether [19], and ii) the magnitude of the Lifshitz–van der Waals force of these coatings that contributed to the total interaction energies is not unambiguous. More notably, the fouling process of calcium phosphate is frequently not a pure crystallization process, but rather in combination with particulate fouling. Such circumstances are experimentally established by Rosmaninho et al. [24]. They showed that the increase in γ^- causes the surface reaction rate coefficient and hence the deposition rate to decrease. Nevertheless, the total deposition rate increased for higher values of γ^- due to the increase of the adhesion coefficient of suspended particulate matter of calcium phosphate. They concluded that the

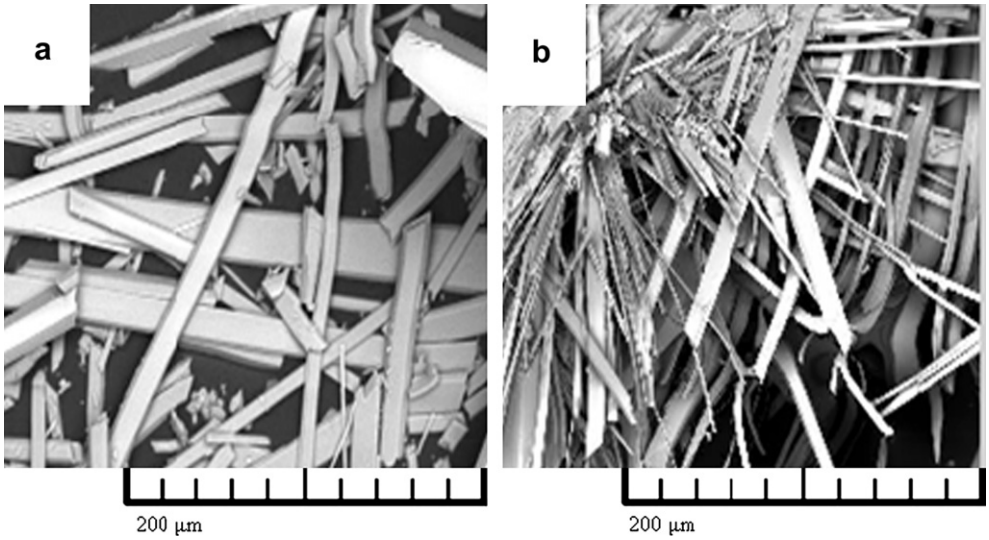

Fig. 11. $CaSO_4$ deposit formed on coated surfaces, a) electroless Ni–P, b) electroless Ni–P–BN (SEM pictures 22.36 μm × 22.36 μm).

adhesion coefficient of particulate matter seems to be the dominant factor in the deposition process rather than the surface reaction rate. Such argument, however, is not valid in this investigation which is deliberately limited to crystallization fouling as the filter depicted in Fig. 4 removes any particles before they may reach the heat transfer specimen.

Visual examination of the fouled surfaces as depicted in Fig. 10 indicates that the Ni–P–BN coated surface has a fragile and thin deposit layer, while for Ni–P and untreated stainless steel surfaces the fouling layer was relatively thick. In comparison, the deposit adhesion on the Ni–P–BN coated surface was less strong than on the Ni–P coated surface. The strongest adhesion of the deposit layer has been observed for the untreated stainless steel surface.

4.2. Deposit morphology

Fig. 11 depicts two typical SEM pictures for Ni–P and Ni–P–BN surfaces for a run with 4 g/L $CaSO_4$ solution and a heat flux of 100 kW/m^2. To obtain such pictures, samples of deposit have been taken at the end of the experiments with great care to avoid any damage to the deposit structure. It was found that the structure of the calcium sulphate deposit is significantly influenced by the type of coating on which the precipitation run has been conducted.

Both crystalline deposits exhibit a needle-shaped structure, which is a typical feature of calcium sulphate dehydrate. However, crystals on the Ni–P–BN surface are thinner and longer compared to those on the Ni–P surface. Longer crystals such as those for Ni–P–BN are probably due to longer induction periods, since a longer induction period allows time for the growth of longer crystals while a shorter induction period favours shorter crystals [25].

Furthermore, both stainless steel and Ni–P surfaces exhibit similar thermal fouling trends, but the crystals on the Ni–P surface were found to be loosely attached to the surface. These crystals can easily be washed away by scrubbing the surface with diluted HCl solutions. Finally a few spots of oxidization have been seen on the surface coated with Ni–P–BN.

4.3. Reproducibility tests

Repeated fouling runs under identical conditions are required to examine if the performance of a modified surfaces is consistent or

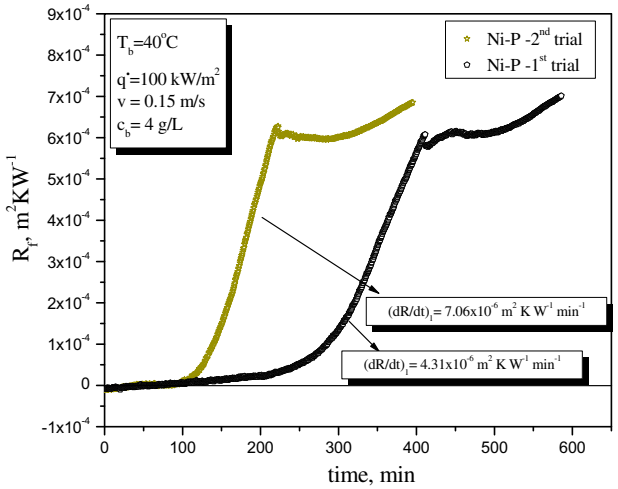

Fig. 12. Reproducibility of the electroless Ni–P coating.

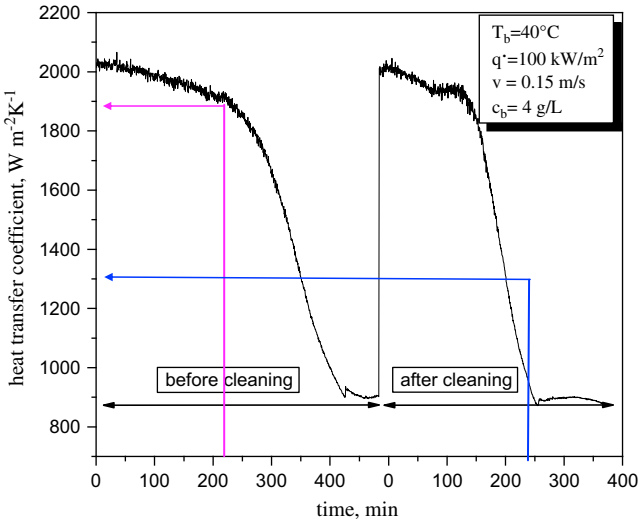

Fig. 13. Heat transfer coefficient versus time for two identical trails of the electroless Ni–P coating.

differs from one run to another. Accordingly, the coated surface was cleaned with 0.05 M HCl (Hydrochloric acid) solution. Afterwards, it was reused for fouling tests under similar operation conditions. The results shown in Fig. 12 indicate that the Ni–P surface demonstrates approximately similar crystallization fouling behaviour in terms of fouling resistance, but slightly higher fouling rate and undoubtedly lower induction time for the second trial. The change of surface roughness after the first run and possibly changes in coating thickness account for such differences. Unfortunately, it was difficult to re-use the Ni–P–BN coated surface for a reproducibility test as signs of oxidization and erosion were spotted after the initial fouling runs.

In addition, Fig. 13 demonstrates the variation of heat transfer coefficient versus time for repeated test shown in Fig. 12. It is obvious that for the Ni–P surface, the heat transfer coefficient has similar trend for both tests i.e. reducing heat transfer coefficient with time. Nevertheless, for a given time for trails, the performance of the Ni–P surface deteriorates substantially after cleaning process. For instance in Fig. 13 after 200 min, the heat transfer coefficient is considerably reduced between the two trails.

5. Conclusions

The formation of calcium sulphate deposits on electroless Ni–P coatings with and without Boron-nitride was investigated and compared with that on stainless steel surfaces. The fouling experiments showed that the deposition process is strongly affected by altering the surface properties, particularly increasing the electron donor component (γ^-) in the case of Ni–P–BN. This is due to the increase in Lewis acid-base energy component of the total interaction energy that increased sharply from stainless steel to Ni–P–BN while the change in Lifshitz–van der Waals energy is negligible. The fouling rate of the electroless Ni–P coatings is lower than that for the untreated stainless steel surface. However among the investigated surfaces, the most significant reduction of fouling rate and longer induction time has been observed for the electroless Ni–P–BN surface. The main drawback with such coating is the poor abrasion characteristics, as some spots of oxidization have been observed after the experiments. In addition, the effectiveness of Ni–P coating to transfer the heat decreases after the cleaning process.

Acknowledgements

The authors gratefully acknowledge the financial support of the European project MEDESOL (The European Commission, Contract no. 036986). The first author wishes also to express his gratitude to the DAAD, "German Academic Exchange Service" for a research studentship.

References

[1] H. Müller-Steinhagen, R.M. Malayeri, A.P. Watkinson, Recent advances in heat exchanger fouling research, mitigation, and cleaning techniques. Heat Transfer Engineering 28 (2007) 173–176.
[2] B.H. Rankin, W.L. Adamson, Scale formation as related to evaporation surface conditions. Desalination 13 (1973) 63–87.
[3] M. Förster, M. Bohnet, Influence of the interfacial free energy crystal/heat transfer surface on the induction period during fouling. International Journal of Thermal Science 38 (1999) 944–954.
[4] S.S. Tulsi, Composite PTFE–nickel coatings for low friction applications. Finishing 7 (1983) 14–18.
[5] Q. Zhao, Y. Liu, S. Wang, Surface modification of water treatment equipment for reducing $CaSO_4$ scale formation. Desalination 180 (2005) 133–138.
[6] N. Krasteva, V. Fotty, S. Armyanov, Thermal stability of electroless NIMEP amorphous-alloys. Journal of Electronic Materials 141 (1994) 941–946.
[7] Q. Zhao, Y. Liu, C. Wang, S. Wang, H. Müller-Steinhagen, Effect of surface free energy on the adhesion of biofouling and crystalline fouling. Chemical Engineering Science 60 (2005) 4858–4865.
[8] T. Young, An Essay on the Cohesion of Fluids, vol. 95, Philosophical Transactions of the Royal Society, London, 1805, pp. 65–87.
[9] C.J. van Oss, R.J. Good, M.K. Chaundhury, The role of van der Waals forces and hydrogen bonds in 'hydrophobic interactions' between biopolymers and low energy surfaces. Journal of Colloid and Interface Science 111 (1986) 378–390.
[10] C.J. van Oss, R.J. Good, M.K. Chaundhury, Additive and nonadditive surface-tension components and the interpretation of contact angles. Langmuir 4 (1988) 884–891.
[11] J.W. Mullin, Crystallization, third ed. Butterworth-Heinemann, Oxford, 1993.
[12] R. Oliveira, Understanding adhesion: a means for preventing fouling. Experimental Thermal and Fluid Science 14 (1997) 316–322.
[13] C.J. van Oss, Interfacial Forces in Aqueous Media. Marcel Dekker, New York, 1994.
[14] C.J. van Oss, R.J. Good, M.K. Chaundhury, Determination of the hydrophobic interaction energy-application to separation processes. Separation Science and Technology 22 (1987) 1–24.
[15] Y. Liu, Q. Zhao, Influence of surface energy of modified surfaces on bacterial adhesion. Biophysical Chemistry 117 (2005) 39–45.
[16] C. Wang, Q. Zhao, Y.L. Liu, Bacterial adhesion mechanism by thermodynamic approach, in: Proceedings of International Federation for Medical and Biological Engineering – 3rd European Medical & Biological Engineering Conference, vol. 11, 2005, pp. 1508.
[17] W. Marshall, R. Slusher, E.V. Jones, Solubility and thermodynamic relationships for $CaSO_4$ in NaCl–H_2O solutions from 40 °C to 200 °C, 0 to 4 Molal NaCl. Journal of Chemical and Engineering Data 9 (1964) 187–191.
[18] G. Rizzo, Induktionszeit beim Kristallisationsfouling an Ionenimplantierten W ärmeübertragerflächen. PhD dissertation, ITW, University of Stuttgart, Germany, 2008.
[19] H. Visser, Improvement of construction materials used in the food industry to lengthen processing time – a new European project (MODSTEEL), in: Proceeding, 4th International Conference on Heat Exchanger Fouling and Fundamental Approaches and Technical Solutions. Davos, Switzerland, 2001, pp. 3–10.
[20] W. Wu, G.H. Nancollas, Kinetics of heterogeneous nucleation of calcium phosphate on anatase and rutile surfaces. Journal of Colloid and Interface Science 199 (1998) 206–211.
[21] W. Wu, H. Zuang, G.H. Nancollas, Heterogeneous nucleation of calcium phosphate on solid surfaces in aqueous solution. Journal of Biomedical Materials Research 35 (1997) 93–97.
[22] R. Rosmaninho, L.F. Melo, Calcium phosphate deposition from simulated milk ultrafiltrate on different stainless steel-based surfaces. International Dairy Journal 16 (2006) 81–87.
[23] R. Rosmaninho, H. Visser, L.F. Melo, Influence of the surface tension components of stainless steel on fouling caused by calcium phosphate. Progress in Colloid and Polymer Science 123 (2004) 203–209.
[24] R. Rosmaninho, F. Roch, G. Rizzo, H. Müller-Steinhagen, L.F. Melo, Calcium phosphate fouling on TiN-coated stainless steel surfaces: role of ions and particles. Chemical Engineering Science 62 (2007) 3821–3831.
[25] R. Sheikholeslami, H.W.K. Ong, Kinetics and thermodynamics of calcium carbonate and calcium sulphate at salinities up to 1.5 M. Desalination 157 (2003) 217–234.
[26] M. Förster, M. Bohnet, Modification of molecular interactions at the interface crystal/heat transfer surface to minimize heat exchanger fouling. International Journal of Thermal Science 39 (2000) 697–708.